

pubs.acs.org/journal/abseba Article

Design and Production of Customizable and Highly Aligned Fibrillar Collagen Scaffolds

Cassandra L. Martin, Chenxi Zhai, Jeffrey A. Paten, Jingjie Yeo, and Leila F. Deravi*



Cite This: https://doi.org/10.1021/acsbiomaterials.1c00566



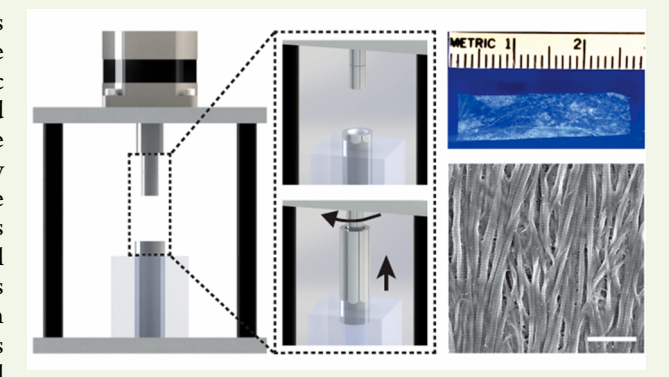
ACCESS

III Metrics & More

Article Recommendations

Supporting Information

ABSTRACT: The ability to fabricate anisotropic collagenous materials rapidly and reproducibly has remained elusive despite decades of research. Balancing the natural propensity of monomeric collagen (COL) to spontaneously polymerize *in vitro* with the mild processing conditions needed to maintain its native substructure upon polymerization introduces challenges that are not easily amenable with off-the-shelf instrumentation. To overcome these challenges, we have designed a platform that simultaneously aligns type I COL fibrils under mild shear flow and builds up the material through layer-by-layer assembly. We explored the mechanisms propagating fibril alignment, targeting experimental variables such as shear rate, viscosity, and time. Coarse-grained molecular dynamics simulations were also employed to help understand how initial reaction conditions including chain length, indicative of initial



polymerization, and chain density, indicative of concentration, in the reaction environment impact fibril growth and alignment. When taken together, the mechanistic insights gleaned from these studies inspired the design, iteration, fabrication, and then customization of the fibrous collagenous materials, illustrating a platform material that can be readily adapted to future tissue engineering applications.

KEYWORDS: collagen, protein, concentric cylinders, fibril alignment, Couette flow, nanofibers

■ INTRODUCTION

The extracellular matrix (ECM) is a complex, multicomponent network that provides the mechanical strength, instructional cues, and underlying structure of tissues and organs in the body.^{1,2} These networks are customized for region-specific architectures, where fiber diameter and organization directly influence tissue form and function. 1,3 For example, the human Achilles tendon contains uniaxial fibrils made of type I collagen (COL) that resist failure under load, withstanding forces and stresses up to ~5000 N and ~80 MPa, respectively. 3-5 On the other hand, the cornea, also comprised of type I COL fibrils but organized as perpendicular sheets, withstands the intraocular pressure in the eye (~1900 Pa) while maintaining optical transparency. 6-9 In an even different manner, the type I COL fibrils in the skin are organized as a woven network that enables the fibrils to straighten, reorient, and slide past each other in order to resist tearing and to redistribute external forces. 10,11 Given the range of unique structure-dependent functions of precisely aligned COL fibrils in vivo, efforts have been made to recapitulate these features in vitro. Applications of blended ECM-based proteins and proteoglycans, such as Matrigel, 12-14 and separated proteins and proteoglycans, 15-18 as well as combinations of these biomolecules with COL, 18,19 have demonstrated the broad appeal for protein-based fibrous

materials in designing engineered tissue. However, it remains technically challenging to generate and scale pure COL fibers. This may be due in part to the fact that the underlying mechanisms regulating COL fibrillogenesis *in vivo*, specifically the use of auxiliary biomolecules, ^{19,20} complex fluid dynamics, ²¹ and cell-matrix tension ²² as critical contributors to this process, are not well understood.

Despite these challenges, there have been several attempts to generate aligned COL scaffolds. One common approach involves extruding concentrated COL as fibers or films with the aid of external electric fields (electrospinning), ^{23,24} centrifugal forces (rotary jet spinning), ¹⁷ differential solvent baths (wet spinning), ^{25,26} or 3D printing. ^{27,28} These extrusion-based methods have demonstrated some potential for scalability in materials applications. For instance, Lee et al. illustrated scalability by 3D-printing a 55 × 37 mm² replicate of a neonatal human heart comprised solely of COL. ²⁷ In spite of

Special Issue: Engineering Bioinspired and Biological

Materials

Received: April 26, 2021 Accepted: August 30, 2021



this incredible feat, it is unclear whether the fibrillar ultrastructure or arrangement of the monomers of the COL fibers was retained throughout this process. The most common approach for generating COL fibers at similar scales is electrospinning; however, this technique is met with some controversy in the field, as data suggests that COL is susceptible to denaturation during the spinning process.^{29–31} When retention of ultrastructure is emphasized, it has often been done so at the cost of scalability. For instance, Saeidi et al. demonstrated that shear flow can align single COL fibrils during the polymerization process in the direction of the flow.³² Other techniques including microfluidics,³³ flow-induced crystallization,²¹ differential electrochemistry,³⁴ magnetic orientation,³⁵ spin coating,³⁶ and nanolithography³⁷ have seen moderate successes in generating and aligning COL fibrils. However, the majority of these procedures lack a realistic pathway to scaling into full tissue replicates and remain limited to producing individual sub-micrometer diameter fibrils or single, long, micrometer-sized fibers.

To improve scalability without sacrificing fibrillar ultrastructure, many researchers have focused on reorienting and aligning preassembled fibrils with the aid of magnetic beadinduced alignment, ^{38,39} biaxial gel compression, ⁴⁰ or counterrotating extrusion. ^{41,42} Perhaps the most readily scalable of the three is counter-rotating extrusion, which was originally designed and utilized to prepare synthetic sausage casings but has since been adapted for tissue engineering applications. 41-44 This method consists of concentric cones rotating in opposite directions, effectively molding a preformed COL dough into sheets, where the shear from the cones is proposed to pull the COL fibrils into a uniaxial alignment. Yang et al. and Hoogenkamp et al. describe collagenous materials with aligned fibers that persist over centimeter-scale lengths, which are at least ten times greater than the other previously mentioned strategies. 41,42 Lastly, the authors describe the utility of these molded scaffolds in a rat Achilles tendon surgery, illustrating their potential in promoting tenogenic differentiation for tendon repair. 42 Despite these successes, the process of counter-rotating extrusion still requires lengthy pre- and post-processing steps in order to both form and retain the initial material geometry. Furthermore, the longer-term impact of the intensive remodeling and restructuring on the integrity and mechanics of the scaffold is still unknown.

We asked whether it would be feasible to reconfigure the counter-rotating extrusion approach to eliminate the need for both a preformed COL dough as a starting material and the salt precipitation steps to "set" the constructs once they have been formed. To test this, we designed a device that consists of two concentric cylinders: a rotating inner cylinder and an outer stationary cylinder that also performs as a reservoir containing the protein solution. In this configuration, the system employs Couette flow to a starting solution, in our case, a monomeric COL solution, that then simultaneously polymerizes and aligns under shear fluid flow to create aligned, continuous fibrous scaffolds. We explore the effect of shear stress, shear rate, and initial polymerization time on COL fibril anisotropy and describe underlying mechanisms potentiating this alignment and subsequent stability without the need for additional postprocessing steps. In support of these goals, we applied and iterated an extensively validated coarse-grained (CG) molecular dynamics model 45-48 to understand how growing chains of COL molecules (indicative of polymerized protein) or groups of COL molecules (indicative of concentrated protein) behave in the presence of flow. The foundation and application of the CG model has been validated for COL molecules and bundles that experience tension, ^{45,46,49-53} shear, ^{46,51} compression, ⁵¹ and cross-link-related properties, ^{45,50} making it an important platform to help understand the events preceding fibril growth and subsequent alignment in our reaction chamber. Finally, given the simplicity of the system, we demonstrate scalability across three dimensions. The primary rate limiting step in this process remains increasing the thickness of the scaffold; however, this challenge can be overcome by adding material via systematic layering events. One feature of this multilayering approach is that the alignment of underlying formed fibrils appears to template the alignment of the subsequent fibril layer, illustrating a facile approach that is amenable to designing, building, and scaling fibrous COL scaffolds *in vitro*.

MATERIALS AND METHODS

Preparation of the Sacrificial Gelatin Coating for the COL Scaffold. A 10% (w/v) solution of gelatin (Electron Microscopy Sciences, 9000-70-8) was prepared in diluted phosphate buffer saline (1× PBS) via stirring and heating at 37 °C. Once dissolved, the solution was heated to 45 °C in a water bath, and the spindle was dipped into the gelatin. The spindle was then attached to the motor and spun sideways at 100 rpm for 10 min to generate a smooth coating.

Preparation of COL Solutions. Acetic acid-extracted bovine type I collagen (Advanced Biomatrix 5026-1KIT) was mixed and neutralized with concentrated phosphate buffer saline ($10 \times PBS$) and sodium hydroxide for a final concentration of either 2.5, 1.5, or 0.5 mg/mL. The COL solution was pH adjusted to 7.3 ± 0.1 using 0.1 M sodium hydroxide and diluted to the desired concentration using distilled water. An overview of COL and COL polymerization *in vitro* is provided in Figure S1.

Preparation of the COL Scaffold. A 0.6 mL solution of the neutralized COL was pipetted into the protein reservoir, and the gelatin-coated spindle was positioned into the center of the chamber and submerged in the solution. The motor was turned on to the desired speed, and the solution was left to spin until the COL completely polymerized at room temperature (Figure S2). The process was consistently performed at 21 °C ± 2 °C so the gelatin would remain solid during the procedure. Afterward, the reservoir was lowered, and the remaining solution was removed. This whole process was done five times to build up the scaffold. A vertical incision was then made to remove the scaffold from the spindle. The spindle was then submerged in a 37 °C 1× PBS solution to dissolve the sacrificial gelatin layer (Figure S3). For materials that were prepared under no shear, the collagen was allowed to polymerize in the reservoir while the spindle remained stationary. Multiple spin cycles were not required for this process, as the COL fibrils formed as mass at the bottom of the reservoir that was easy to transfer. Throughout all experiments, a negligible amount of evaporation occurred during a single spin cycle (<0.01%), suggesting the humidity of the surrounding environment should not significantly impact the final

Scanning Electron Microscopy (SEM) Preparation and Imaging. The scaffold was laid flat onto an aluminum SEM stage coated with carbon tape. The side of the scaffold that was facing out toward the solution was face-up on the stub. The scaffold was airdried overnight, sputter coated with 2.5 nm of platinum, and then imaged with a SEM (Hitachi, S-4800) to show the fibril organization in the scaffold. Five representative images were taken at different locations of each scaffold to both obtain an accurate fibril alignment measurement of the scaffold and ensure uniform fibril alignment throughout the scaffold.

To prepare the scaffolds for thickness measurements, the samples were cross-linked using 2.5% (v/v) glutaraldehyde (in 1× PBS) and then buffer-exchanged by replacing half of the solution volume with

1× PBS solution seven times. They were then dehydrated in 95% ethanol through a graded series of solution exchanges. A glass coverslip was placed in the ethanol under the scaffold, and the ethanol was then left to evaporate in a fume hood, which caused the material to dry onto the glass coverslip. The coverslip with the scaffold was then submerged in liquid nitrogen and fractured lengthwise down the scaffold. The pieces were sputter coated with 2.5 nm of platinum before SEM imaging. Three scaffolds were prepared for each condition (three, five, and seven layers), and five images were taken of each scaffold.

Fibril Alignment Analysis. Each SEM image was analyzed via a MATLAB code designed by Dr. Edward A. Sander that measures the fibril distribution in an image. ⁵⁴ Before analysis, the SEM image was first cropped into a square for the most accurate analysis. Then, the Fourier transform filters were adjusted. In summary, the upper Fourier transform filter in the MATLAB code was adjusted by measuring the average fibril diameter (10 measurements) in the image, doubling the value, and converting it to a frequency value based on the dimensions of the image (eq 1). This value was then increased by 10% to improve the accuracy of the analysis and adjusted to a filter value unique for the code (eq 2). The lower Fourier transform filter was held constant due to a negligible effect on the overall results.

$$frequency = \frac{pixel \ width \ of \ image}{(2 \times average \ fibril \ diameter)} \tag{1}$$

$$filter = \frac{adjusted frequency}{pixel width of image}$$
 (2)

This code first converts the square image to the frequency domain with the fast Fourier transform method and then into polar coordinates. The program then determines the number of points that contribute to each angle between 0 and 360° and measures the frequency of each angle in the image. The orientation tensor was also calculated for each image. With this data, we determined the percentage of fibrils that fell within $\pm 20^{\circ}$ of the calculated orientation tensor of the overall image. For each trial, five images were analyzed and averaged over three independent scaffolds. The error was reported as plus or minus the standard deviation.

Computational Methods. In our investigation, the solvated tropocollagen molecules are modeled as a number of beads with multibody potential interactions of 1–1.5 amino acids, which corresponded to 10–20 atoms. This CG model was derived from a high-fidelity AA triple helical tropocollagen model generated from Protein Data Bank entry 3HR2 type I COL⁵⁵ to enable simulations at larger time and length scales (see SI for full details). ⁴⁶ The initial configuration of the beads was spaced at 14 Å at equilibrium, which was close to the diameter of a COL molecule. ^{46,56} The parameters are fully given in Table S1, such that the fluid shear is being handled within this implicit-solvent potential force field. The tethering is handled by applying a point force at one end of the tropocollagen, mimicking the starting condition, where a single tropocollagen adheres, or *tethers*, to gelatin during spinning (see SI for full details).

Our simulation box was set to be longer than a molecule to avoid interactions between opposing ends of the same chain due to the periodic boundary conditions. The paired potentials of the interacting beads in the CG model were described with a Lennard-Jones (LJ) style interaction in eq 3:

$$E_{\text{paired}} = 4\varepsilon_{\text{LJ}} \left[\left(\frac{\sigma_{\text{LJ}}}{r} \right)^{12} - \left(\frac{\sigma_{\text{LJ}}}{r} \right)^{6} \right]$$
(3)

where $\varepsilon_{\rm LJ}=11.06$ kcal/mol was the dispersion energy and $\sigma_{\rm LJ}=14.72$ Å was the equilibrium distance between two interacting beads where the LJ potential energy was zero. This force field and associated parameters are derived from AA models and are validated in a series of publications. $^{46,49-51}_{46,49-51}$ The bonded interaction in this model was described using eq 4:

$$E_{\text{bonded}} = \begin{cases} k_1 (r - r_0)^2, & r < r_1 \\ k_2 (r - r_0)^2, & r_{\text{break}} > r > r_1 \\ 0, & r > r_{\text{break}} \end{cases}$$
 (4)

where $k_1 = 17.13$ (kcal/mol)/Ų and $k_2 = 97.66$ (kcal/mol)/Ų were the spring constants in small and large strains, $r_0 = 14$ Å was the equilibrium distance of the spring, $r_1 = 18.2$ Å was the critical hyperelastic distance, and $r_{\text{break}} = 21$ Å was the bond breaking distance. The angular potential was calculated using eq 5:

$$E_{\text{angular}} = k_{\text{angular}} [\beta - \beta_0]^2 \tag{5}$$

where the bending stiffness was represented as $k_{\rm angular} = 14.98$ (kcal/mol)/rad² and the equilibrium angles were represented by β_0 values ranging between 170° and 180°.

The local chain alignment at each bead i was described using a vector $\mathbf{e}_i = \frac{r_{i+1} - r_{i-1}}{|r_{i+1} - r_{i-1}|}$. Therefore, we used the alignment parameter, P_2 , which was calculated using eq 6 as

$$P_2 = \frac{\sum_{i=1}^{N} 3(\mathbf{e}_i \cdot \mathbf{e}_{\text{shear}})^2 - 1}{2N}$$
(6)

This value was calculated to described the orientation of the molecule along the shearing direction, where $\mathbf{e}_{\text{shear}}$ was the unit vector along the shear direction and N represented the total number of beads (see SI for full details). 57,58

In all calculations, COL molecules were equilibrated for 2 ns before the shear, and the shear simulations were run for enough time until the P_2 value reached a steady state, indicating that the system was in equilibrium. All the simulations were performed using the canonical ensemble (NVT, where the moles, volume, and temperature in the system are conserved). ⁵⁹

Scaffold Thickness Analysis. The thickness of the scaffolds was determined from the cross-section SEM images using ImageJ. Fifteen measurements were taken for each independent sample across five fields of view. Each condition consisted of three independent samples. The average thickness and the standard deviations of each condition were calculated from these measurements.

Statistical Analysis. Statistical analysis was completed in Microsoft Excel with a one-way ANOVA test where the p-value equals 0.05. The null hypothesis stated that there was no significant difference between the tested conditions. In the analysis, if $F > F_{\rm crit}$, then at least one condition was different from the other conditions, and the null hypothesis was rejected. To determine which conditions were different from each other, a Tukey test was performed, where two sets of values were directly compared, and the p-value was equal to 0.05.

To compare the fibril alignment of our $3.0 \times 1.0 \text{ cm}^2$ scaffold to the $4.5 \times 1.5 \text{ cm}^2$ scaffold, a paired t test was completed in Microsoft Excel. The p-value was set equal to 0.05. Results less than 0.05 indicated that the alignment in the scaffolds were significantly different from each other.

RESULTS

Formation of Anisotropic COL Scaffolds. To generate sheets of COL fibrils, we designed and built a device with two concentric cylinders, where the inner cylinder (the spindle) rotated, and the outer cylinder (the reservoir) remained stationary (Figure 1A); the gap space between the two cylinders remained constant at \sim 1 mm. This setup allowed for neutralized COL to spontaneously polymerize under shear flow, leading to the formation of a fibrillar scaffold (Figure 1B and Figure S3). Prior to spinning, the spindle was coated with a uniform layer of un-cross-linked gelatin with a thickness of 28.3 \pm 5.0 μ m, where the gelatin acts as a surface for the collagen to adhere, or tether, during fibrillogenesis (Figure S4). Without the gelatin layer, polymerized COL formed only as a

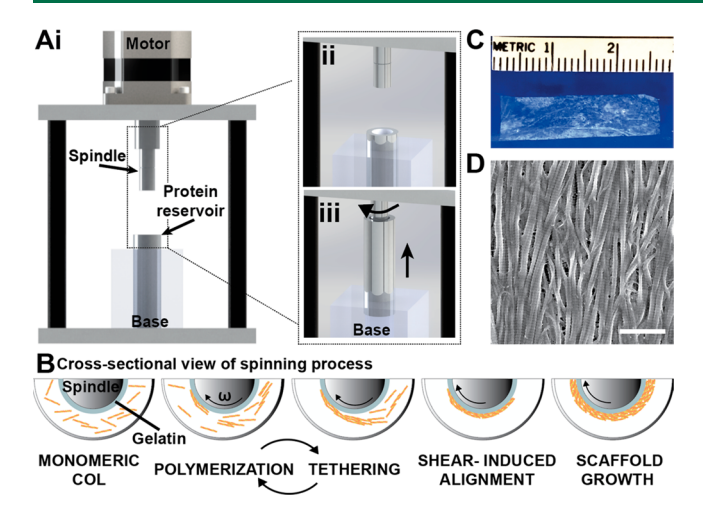


Figure 1. Development of highly aligned COL scaffolds under Couette flow. (A) Complete platform, where (i) COL scaffolds were generated with a custom-built device composed of two concentric cylinders. Top cylinder (spindle) was connected to a motor and rotated, and bottom cylinder (protein reservoir) could be (ii) lowered and (iii) raised to disengage or engage the system. The spindle is 25.2 mm long (but only ~14 mm gets submerged in the reservoir) and 10.6 mm in diameter. The reservoir is 15.2 mm deep and 12.6 mm in diameter. (B) The spinning process involves multiple steps where monomeric COL simultaneously polymerizes and tethers to the thin, sacrificial layer of gelatin. (C) After spinning, a ~3.0 \times 1.0 cm² scaffold was collected off the spindle, where (D) the resultant fibrils have high alignment and the signature D-banding of fibrillar COL as seen in the representative scanning electron microscope image. Scale bar = 2 μ m.

thin strip at the air-liquid interface (Figure S4A); furthermore, if no shear is present during fibrillogenesis, then no fibrils form on the gelatin-coated spindle. These observations point to a synergistic relationship between the assembling COL solution and the gelatin interface, which we believe is required to initiate adhesion of monomers, nucleation of fibrils, and ultimate generation of a continuous fibrous material. In the presence of the gelatin, COL fibrils spanned the entire spindle length, enabling their collection as a $\sim 3.0 \times 1.0 \text{ cm}^2 \text{ scaffold}$ with a porosity of only 4.9% ± 2.1%, highlighting the tightly packed nature of the fibrils (Figure 1C, Figure S4B, and Figure S5). Perhaps more importantly, the gelatin served as a sacrificial layer that allowed for an easy removal of the scaffold from the spindle without disrupting the anisotropic substructure. The presence of native D-banding on the COL fibrils indicated that the shear-induced alignment did not disrupt the natural polymerization of COL (Figure 1D); the bands had an average width of 65.5 ± 3.6 nm, which is comparable to band widths published in the literature, and the D-banding that was imaged on a rat tail tendon (Figure S6). Furthermore, the exquisite fibril alignment, uniform D-banding, and consistent fibril diameters that persisted throughout the scaffolds were comparable to those found in isolated rat tail tendons, but the fibril alignment in the scaffolds differed significantly from fibrils formed in a COL gel in the absence of shear (Figure 2A-C, and Figure S6). We calculated that $74.0\% \pm 3.2\%$ of the shearaligned fibrils were within $\pm 20^{\circ}$ of the orientation of all fibrils in the scaffold. This alignment was statistically similar to the 77.7% ± 7.9% alignment calculated from fibrils in an isolated rat tail tendon specimen and significantly differed from the scaffold formed with no shear (Figure 2D). Despite how they

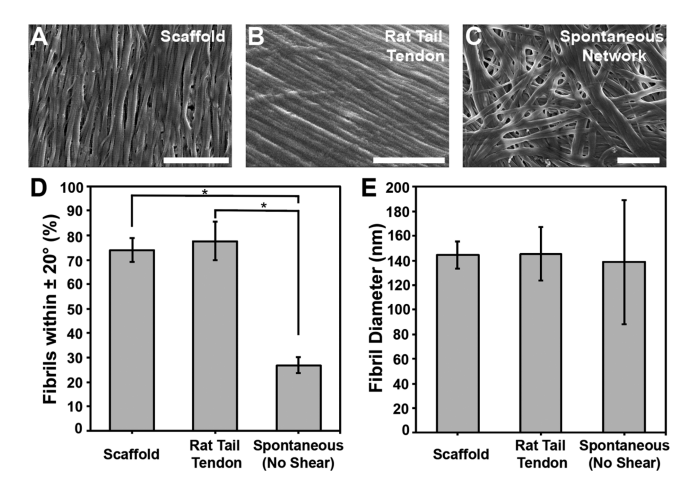


Figure 2. Comparison of the COL scaffolds to rat tail tendons and COL gels spontaneously formed with no shear. Representative SEM images of (A) a five-layered COL scaffold prepared with 2.5 mg/mL COL and spun at $75 \, \text{s}^{-1}$, (B) a rat tail tendon, and (C) a fibrous COL gel that spontaneously polymerized under no shear. (D) Fibril alignment was determined by measuring the percentage of fibrils that fell within $\pm 20^\circ$ of the orientation tensor for the image. In this analysis, n=15, where five measurements were taken on three independent samples and error is reported as $\pm \text{SD}$ (standard deviation). (E) Variation of fibril diameter for each structure, where n=300 fibrils over three independent samples and error is reported as $\pm \text{SD}$. Statistically significant differences for both sets of results are denoted with an asterisk where p<0.05. Scale bars $=2 \, \mu \text{m}$.

were made, fibril diameters remained consistent in each sample, indicating that the shear flow from the device did not inhibit the natural polymerization process (Figure 2E).

Analysis of the Mechanism behind Fibril Alignment. After examining the effects of both shear and the presence of the gelatin layer on the formation and alignment of COL fibrils, the next goal was to look at the effect of these variables on individual COL molecules in parallel to the full fibers. The goal was to gain insight into the mechanism behind the COL fibril alignment that is observed by examining the initial effect that shear flow had on the COL monomers before fibril formation. To further examine the impact of tethering on the dynamic alignment of COL molecules under shear, a CG simulation framework was constructed to qualitatively simulate molecules as beads, where one bead experienced a tethering force at the end of the chain. Here, we define tethering force as the anchoring force that keeps one end of the molecule stationary, such that the molecule only experiences application of a uniaxial force. In this configuration, our simulations emulated the initial deformation of the COL molecules experiencing this tethering force, which we defined as the uncoiling and alignment of the molecules on the spindle.⁴⁹ To determine if our molecules aligned in the direction of the applied force, we calculated the uniaxial order parameter, or P_2 , value in the system. 57,58 Under these conditions, we observed that a single COL molecule gradually aligned within approximately 3 ns when the magnitude of the tethering force was above 0.005 (kcal/mol)/Å (Figure 3A, i). When the tethering force was below this threshold, the simulated COL did not overcome the pairwise, long-range cohesive/attractive forces between two interacting beads, resulting in an unaligned structure (Figure S7). Above this threshold, the tethering force could surmount these opposing forces and initiate the

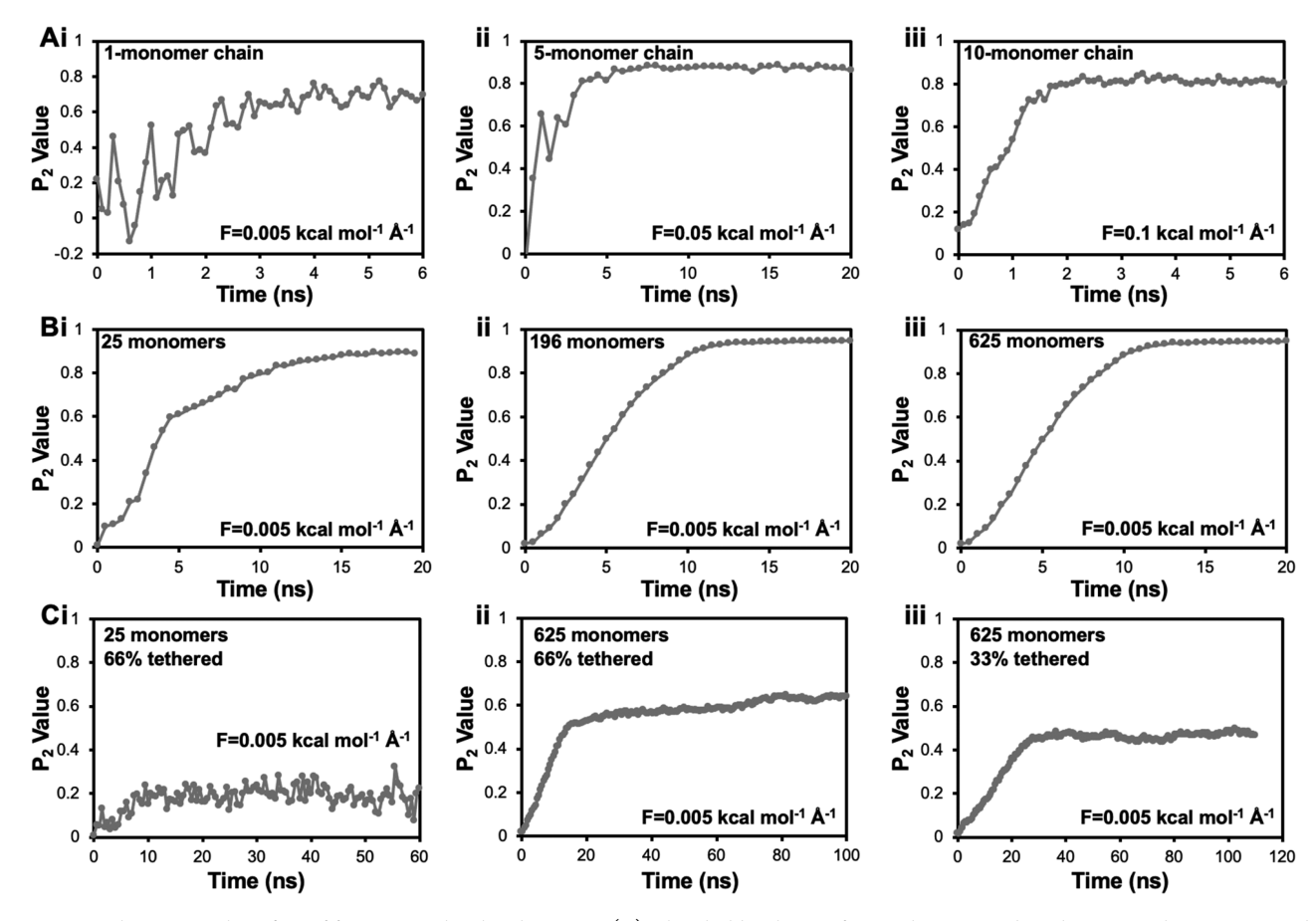


Figure 3. Evaluation on the effect of force on molecular alignment. (A) Threshold tethering force value required to align COL chains composed of (i) 1, (ii) 5, and (iii) 10 molecules in the direction of the flow. Results show that as the chain length increased, the amount of force required to achieve a high P_2 value increased. (B) When the number of COL monomers increased from 1 to (i) 25, (ii) 196, and (iii) 625 monomers, the same threshold force value was needed to align all of the molecules in the system. (C) The percentage of molecules that experience the tethering force was shown to influence the final alignment of the system. (i) If only two-thirds of a 25-monomer system was exposed to the force, the molecules were unable to align, highlighting the importance of the tethering. However, in a 625-chain system, (ii) the monomers achieved a certain degree of alignment when two-thirds of the molecules were tethered. (iii) If only one-third of all molecules experienced tethering, the alignment was worse.

uncoiling of the COL molecule, which eventually facilitated overall alignment of the structure. 49

To expand on these findings, we next calculated the threshold force required to align COL chains that were 1, 5, and 10 monomers long. We observed an increase in threshold force as the chain length increased likely due to the larger intramolecular adhesion and pairwise attractive forces that intensified as the number of CG beads increased (Figure 3A). Interestingly, we also found that the minimal force needed to align multiple monomers of COL was the same as that of a single COL molecule, suggesting that the starting COL concentration should not significantly impact alignment (Figure 3B). The intermolecular interactions experienced between multiple chains of the shorter, monomeric COL molecules during shear were beneficial for catalyzing alignment within our system.

We next explored the role of molecular tethering on the overall alignment of the multichained systems. In these studies, we varied the percentage of molecules that experienced tethering and monitored how these changes impacted the P_2 value (Figure 3C). In a system with only 25 COL chains, alignment was worse when 66% of the chains were tethered, as indicated by the low P_2 value (Figure 3C. i). However, we found that overall alignment increased in a 625-chain system when either 100% (Figure 3B, iii) or 66% (Figure 3C, ii) of all

chains were tethered, and misalignment reigned when only 33% of the chains were tethered (Figure 3C, iii). This difference indicated that tethering was necessary for overcoming entropic effects and inducing system-wide alignment within starting solutions consisting of concentrated monomers (e.g., more available chains of shorter COL molecules). Based on these findings, we deduced that a portion of the molecules needed to be tethered to drive scaffold formation and ultimate alignment.

To expand on these results, we monitored effects of prepolymerization (indicative of a growing COL chain) on alignment (Figure 4A-C). In our studies, we delayed the spinning process for 1 and 5 min after triggering COL polymerization and compared changes to alignment with a solution that was simultaneously polymerized under shear (e.g., 0 min delay). Fibril alignment in the scaffold decreased from $74.0\% \pm 4.9\%$ to $64.4\% \pm 13.0\%$ to $40.2\% \pm 12.5\%$ at a 0, 1, and 5 min spin delay, respectively (Figure 4D). These results suggest that the COL fibrils had grown long enough during the delay period, where shear flow was no longer capable of aligning the structure. In each case, there were also no notable changes to fibril diameter (Figure 4E). When the COL was left to polymerize for 10 min before spinning was engaged, the fibrils were unable to adhere to the gelatin coating; instead, they formed a bundle of isotropic fibers at the

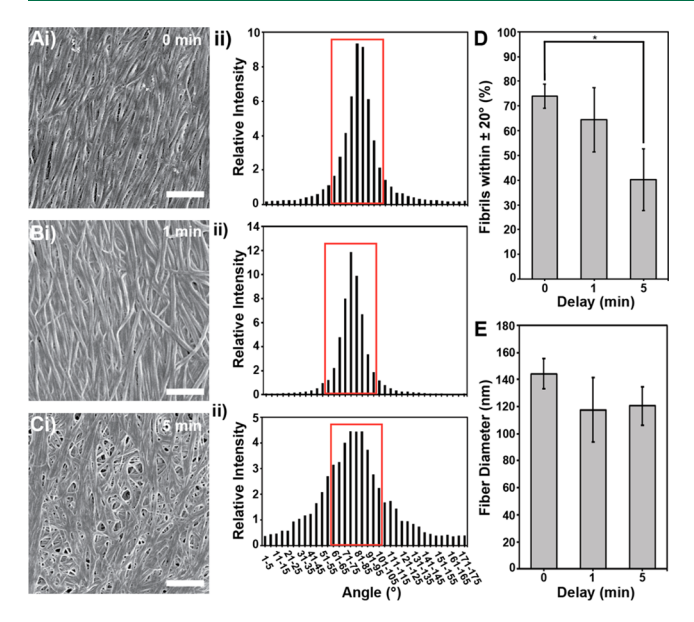


Figure 4. Neutralized COL solution (2.5 mg/mL) was left to partially polymerize while exposed to no shear in the protein reservoir for (A) 0, (B) 1, and (C) 5 min, where (i) SEM images and (ii) measured histograms illustrate the distribution of fibrils formed in each condition. The red boxes in part ii of each panel illustrate the $\pm 20^{\circ}$ range that was utilized to quantify fibril alignment in panel D. In this analysis, n=15, where five measurements were taken on three independent samples and error is reported as \pm SD. (E) Average fibril diameter in the scaffolds for each condition, where n=300 fibrils over three independent samples and the error is reported as \pm SD. For both graphs, an asterisk indicates that the results were significantly different from each other (p<0.05). Scale bar = 2 μ m.

bottom of the reservoir (Figure S8). These results were in agreement with the computational predictions, supporting that the shear force in our system was required to trigger adhesion between the spindle and COL monomers and that partial prepolymerization under no shear decreased the number of tethered COL molecules and fibril alignment. When taken together, our computational and experimental findings suggested that a combination of larger critical forces and longer spinning times would be necessary to align the prepolymerized COL fibers. In summary, both the gelatin tethering layer and simultaneous spinning and polymerization of COL were needed to achieve eventual alignment; without these design features, the resultant material became disordered.

Tuning Shear Rate to Maintain Fibril Alignment. Given the dependence on spin time and tethering capacity on the alignment and growth of the scaffolds, we asked what other variables regulated scaffold formation. Shear rates of 50, 75, and 100 s⁻¹ were first investigated, and we found 69.7% \pm 18.9%, 74.0% \pm 3.2%, and 65.5% \pm 14.8% of fibrils fell within $\pm 20^{\circ}$ of the orientation tensor, respectively, and that the shear rate had no influence of fibril diameter (Figure S9A-C). To establish the maximum shear rate that we could achieve without losing alignment, we also prepared scaffolds at 1000 s⁻¹ and found that the alignment was not significantly different from that in our other scaffolds (Figure S9A(iv),B). This is not surprising, as the calculated Reynolds numbers suggested that the flow produced by the rotating spindle at these shear rates was laminar (Table S2). At shear rates above 1000 s⁻¹, the gelatin coating was torn off the spindle, preventing scaffold formation altogether. Even though the results were not

significantly different from each other, fibril organization was greatest at 75 s^{-1} and was sufficient to induce broad area alignment across the entire scaffold (Figure S10).

Because we observed negligible changes to fibril alignment as a function of shear rate, we next asked if maintaining the shear stress of the system would preserve fibril alignment at multiple concentrations of COL. Because shear stress is directly related to the shear rate and viscosity, we approximated that a constant shear stress of 1.7 N/m² (the amount of shear the system applies at 75 s⁻¹) could be maintained by adjusting the rotational speed for solutions prepared at different concentrations of COL (Figure 5A).

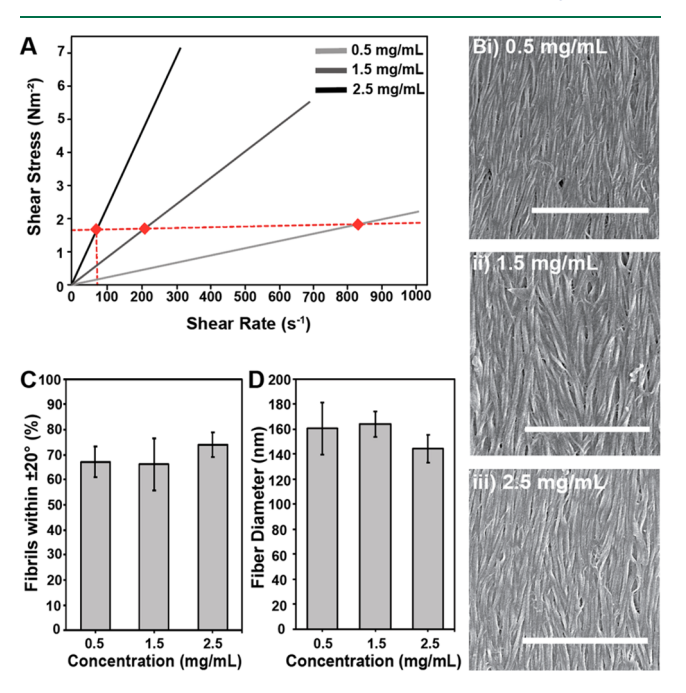


Figure 5. Scaffolds were produced at three concentrations, which generated three distinct viscosity profiles. (A) Shear rate was increased to maintain a constant shear stress in the system. (B) Representative SEM images for (i) 0.5 mg/mL, (ii) 1.5 mg/mL, and (iii) 2.5 mg/mL illustrated the alignment that persisted in each condition, which was also quantified from calculating the percentage of fibrils that fell within $\pm 20^{\circ}$ of the orientation tensor (C). Here, n=15 where five measurements were taken on three independent samples and error is reported as \pm SD. Results in panel D show that neither the varying concentrations of COL nor the increased shear rate significantly influenced fibril diameter, where n=300 fibrils over three independent samples and error is reported as \pm SD. Scale bar = 5 μ m.

When shear stress was maintained, we were able to achieve statistically similar alignment for each condition (67.1% \pm 6.1%, 66.1% \pm 10.4%, and 74.0% \pm 3.2% for 0.5, 1.5, and 2.5 mg/mL, respectively, Figure 5B,C). These findings supported that shear stress was critical to maintaining fibril alignment (Figure 5C) and fibril diameter (Figure 5D) even when other parameters (i.e., shear rate and concentration) were altered.

Increasing Scaffold Dimensions and Composition. To investigate the tunability of this platform, we next varied the dimensions (length, width, and thickness) of the scaffold and measured the impact on fibril alignment. We started by changing the number of COL layers in the scaffold and found that the thickness of dried 3-, 5-, and 7-layered scaffolds (e.g., repetitive spin cycles) increased to 369 ± 73 nm, 625 ± 32 nm,

and 813 ± 76 nm, respectively (Figure 6A,B). It was interesting to note though that when the shear rate was held

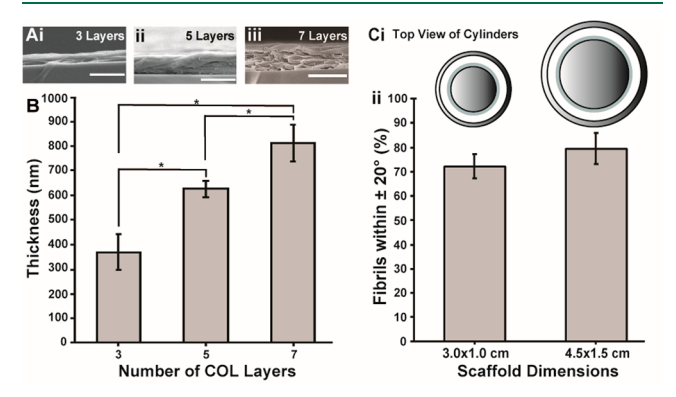


Figure 6. (A) Representative cross-sectional SEM image of a (i) three-, (ii) five-, and (iii) seven-layer COL scaffold. (B) Comparison of the thickness of a three-, five-, and seven-layer scaffolds where results illustrate a significant increase in the thickness of the scaffold, indicating that the scaffold thickness can be increased without negatively influencing fibril organization. The final result is n = 75, where three independent scaffolds were prepared for each condition, and five images were taken of each scaffold. Five measurements were then taken on each image, and the error is reported as ±SD. To increase the length and width of the scaffold, (C, i) a larger device was designed that produced a scaffold with a 50% increase in the length and width of the scaffold compared to the original one. (C, ii) Fibril alignment results indicate that the anisotropic nature of the fibrils was preserved in the larger scaffold. In this analysis, n = 5 where five measurements were taken across a single scaffold and error is reported as ±SD. Results with an asterisk between them indicates a significant difference between values (p < 0.05). Scale bar = 1 μ m.

constant, fibril alignment increased when the number of COL layers increased from 3 to 5, suggesting that previous layers partially templated the alignment of new fibrils (Figure S11). However, there was no significant improvement in fibril alignment between the 5- and 7-layered scaffolds, indicating that the fibril organization is maintained even when the thickness is further increased. Finally, we noted the porosity of the 3- and 7-layered scaffolds remained statistically similar to the previously mentioned porosity of the 5-layered scaffold at $4.1\% \pm 2.0\%$, $4.9\% \pm 2.1\%$, and $3.4\% \pm 1.1\%$ for the 3-, 5-, and 7-layered scaffolds, respectively (Figure S5).

To complement the results from the thickness analysis, we next asked how an increase in the length and width of the scaffolds impacted structure formation and ultimate alignment. To test this, we increased the footprint of the device by 50% in a new design which, as a result, increased the size of the scaffold to approximately $4.5 \times 1.5 \text{ cm}^2$ (Figure 6C, i). This increase in size did not significantly alter the fiber alignment throughout the scaffold when compared to the smaller 3.0 X 1.0 cm² scaffold, indicating that scaling this design was feasible without sacrificing the underlying substructure of the scaffolds (Figure 6C, ii). Finally, we tested whether we could incorporate other fibrillar proteins to diversify the scaffold composition. To test this final variable, we blended soluble fibronectin (FN) into the starting COL solution and prepared the scaffolds. We observed the presence of fibrillar FN that persisted throughout the scaffolds (fluorescently labeled green in Figure S9). To confirm that the FN was indeed in its fibrillar form, we incubated the scaffold in 2% sodium deoxycholate, a chemical that digests globular but not fibrillar FN and observed a FN positive fluorescence signal that indicated its presence in the fibrillar form in the scaffold (Figure S12). When taken together, our findings suggested that our system can be tuned to enable the production of multicomponent and multidimensioned scaffolds; both are important characteristics when considering designs for future tissue engineering applications.

DISCUSSION

We have designed, built, and tested a device that leverages Couette flow to generate shear and align COL as it spontaneously polymerizes under ambient conditions. While the use of shear to align COL fibrils is not new, our approach is among the first to incorporate fluid flow together with dynamic polymerization to align and grow COL scaffolds with anisotropic substructures. Our optimal shear rate of 75 s⁻¹ is comparable to other reports that have generated aligned COL fibrils including Saeidi et al. (20 and 80 s⁻¹), Nerger et al. (100 s⁻¹), and Lai et al. (\sim 200 s⁻¹). ^{13,32,60} Unlike previous work, we validated that proper COL polymerization has occurred through the presence of D-banding along each of our fibrils, where the banding was comparable to those in the rat tail tendons and from native COL fibrils reported in the literature (Figure S6).56 Because our process can simultaneously nucleate, tether, and grow COL fibrils during scaffold formation, these signature anisotropic features with negligible surface defects are retained across the centimeter scale of our materials.

The incorporation of the sacrificial gelatin layer during scaffold formation is another differentiating but essential feature of our platform that not only improved the dimensions and practical handling of the material, but also contributed to fibril alignment during polymerization. COL monomers interact with each other via noncovalent interactions, and we suspect that electrostatic and hydrogen bonding occurs during polymerization; since gelatin is simply denatured COL, it is likely that similar interactions occur during scaffold development.⁶¹ Despite this natural interaction, scaffold formation on the spindle only occurs under shear flow. These findings were further supported by our computational analysis, which suggested that once the molecular alignment process was initiated under flow, it facilitated the uncoiling of neighboring, unaligned molecules via intermolecular repulsion as a result of limited wiggle room. This hypothesis was supported by the steep increase in P2 in Figure 3C, ii, which denoted the structural evolution of the tethered molecules, followed by its gradual increase over time attributed to an increased susceptibility of untethered molecules to align in the presence of the tethered chains. Because we are simulating the single tropocollagen molecule with a concentration calculated to be 0.3×10^{-4} mg/mL, which is about 4 orders of magnitude more dilute than our most dilute experimental COL solution (0.5 mg/mL), we are only simulating the very initial stages of the aligning process to provide some fundamental, qualitative insight compared to the experimental large scale of micro- to millimeters. When taken together with our experimental data, these findings highlighted that molecular tethering is a requirement for alignment. When the start time for spinning the COL was delayed, indicative of a conversion of molecules to fibrils, a lower percentage of molecules could be tethered, making alignment inconsistent and, in some cases, impossible.

The exploration and characterization of the planar fibril structures produced in this report were necessary for understanding the molecular mechanisms underlying scaffold formation; however, the true translatable features of our approach lie its design versatility and compositional customizability, two attributes that we demonstrate in a proof-ofconcept approach in Figure 6. Because the spindle and outer chamber are CAD-based designs, they can be easily reconfigured and scaled to generate multiple shapes and structure. We demonstrated two dimensions of a cylinder, but the design could conceivably be reconfigured to multiple geometries and structures. By systematically increasing the number of spin cycles, we can also increase the thickness of the scaffold while maintaining fibril anisotropy, which has shown to be a critical step in generating a usable material. If the spin cycle is not repeated, it is difficult to both remove and handle the resulting scaffold without causing significant damage. However, performing multiple spin cycles not only adds to the durability of the material but also contributes to fibril alignment (Figure S11). Other researchers have utilized aligned materials, such as dextran fibers and micropatterned glass slides to align COL fibrils during the polymerization process.^{62,63} It is possible that in our system the already polymerized fibers act as a template for polymerizing fibrils and may (1) serve as nucleation sites for further layers or (2) display stronger electrostatic and hydrogen-bonding interactions with the polymerizing COL than the smooth gelatin layer does. Overall, the process of repeating spin cycles is crucial in improving both the durability and alignment of the scaffold. However, the thickness of the scaffolds cannot be scaled to the same degree as the other two scaffold dimensions. Future experiments and modifications focusing on more efficiently increasing the thickness of the scaffold, such as changing the gap distance between the spindle and reservoir, or determining how to adhere two scaffolds together, are necessary to further enhance the utility of this material.

Finally, because scaffold formation is dependent on initial solution viscosity, we can adjust the operating parameters (e.g., shear rate) of our system to account for compositional changes that would enable the addition of other components during fiber formation. We utilized FN as our proof-of-concept molecule, given its ability to unfold under shear and known codependent relationship with COL, to demonstrate that other biomolecules can be integrated into our scaffold along with the COL. Rinsing the FN-COL scaffold in sodium deoxycholate indicated that the FN present in the scaffold was indeed fibrillar. Although the exact alignment of these FN fibers is unknown, there is a plethora of evidence from the literature that suggests that the FN fibers are in alignment with the COL fibrils. For example, Ejim et al. used the shear flow generated from a stirred cell to trigger FN fibrillogenesis and create mats of FN. 15 Results showed that the orientation of the FN fibers was in the direction of the flow, much like the COL fibrils in our material. In addition, Paten et al. demonstrated that in a cell-free environment, collagen polymerization initiated FN fibrillogenesis and, more importantly, that there was a high degree of colocalization between the two protein fibers; since our setup produced highly aligned COL fibrils, it is likely that the FN fibers in the scaffold match the orientation of the COL fibrils. 19 Future studies will be aimed at expanding the repertoire of biomolecules that can be added to these scaffolds while including an assessment of their biological performance in vitro.64,65

CONCLUSIONS

Overall, we have developed a platform that leverages the natural polymerization process of COL to reproducibly generate scaffolds with highly aligned fibril substructures. Parameters in the system such as shear rate, polymerization time, and concentration were explored and adjusted to both optimize the fibril alignment in the material and understand the process behind the uniaxial fibril orientation. Furthermore, we utilized CG molecular dynamics simulations to understand the initial stage of the alignment process where the COL monomers are first introduced to shear flow. Our system is tunable, as it produces structures at multiple dimensions without sacrificing fibril structure and alignment, both of which closely mimic collagenous fibrils from isolated rat tail tendon. Perhaps most interesting is that previous layers of aligned fibrils further improve the alignment of future layers of fibrils up to a degree. Future work consists of developing a more efficient approach to increasing the thickness of the material. Furthermore, while our scaffolds currently consist of layered, type I COL fibrils, preliminary data suggests the immediate potential to incorporate a broad spectrum of biological molecules for tuning the scale and types of tissues formed. These features enable a streamlined pathway to generate customizable materials for future tissue engineering applica-

ASSOCIATED CONTENT

Supporting Information

The Supporting Information is available free of charge at https://pubs.acs.org/doi/10.1021/acsbiomaterials.1c00566.

Additional methods, overview of COL and COL polymerization, COL fibrillogenesis kinetics analysis, illustrated protocol of the steps required to produce aligned scaffolds, analysis and impact of the sacrificial gelatin layer, porosity measurements of COL scaffolds, D-banding analysis of fibrillar COL in various structures, computational analysis of the effect of force on single COL monomer alignment, effect of spinning COL after 10 min of polymerization under no shear, influence of shear rate on fibril alignment and diameter, consistency of alignment throughout the COL scaffold, effect of layering on fibril alignment, incorporation of FN into the COL scaffold, CG simulation framework parameters, and Reynolds numbers of various shear rates in the device(PDF)

AUTHOR INFORMATION

Corresponding Author

Leila F. Deravi — Department of Chemistry and Chemical Biology, Northeastern University, Boston, Massachusetts 02115, United States; orcid.org/0000-0003-3226-2470; Email: l.deravi@northeastern.edu

Authors

Cassandra L. Martin – Department of Chemistry and Chemical Biology, Northeastern University, Boston, Massachusetts 02115, United States

Chenxi Zhai — Sibley School of Mechanical and Aerospace Engineering, Cornell University, Ithaca, New York 14853, United States; Department of Mechanical Engineering, FAMU-FSU College of Engineering, Florida State University,

- Tallahassee, Florida 32310, United States; oorcid.org/0000-0003-2913-3328
- Jeffrey A. Paten Department of Chemistry and Chemical Biology, Northeastern University, Boston, Massachusetts 02115, United States; John A. Paulson School of Engineering and Applied Sciences, Harvard University, Cambridge, Massachusetts 02138, United States
- Jingjie Yeo Sibley School of Mechanical and Aerospace Engineering, Cornell University, Ithaca, New York 14853, United States: Occid.org/0000-0002-6462-7422

Complete contact information is available at: https://pubs.acs.org/10.1021/acsbiomaterials.1c00566

Author Contributions

C.L.M., J.A.P., and L.F.D. designed both the device and experiments and interpreted the results. C.L.M. performed the experiments and analyzed the results. C.Z. and J.Y. designed, performed, and analyzed the computational experiments. All authors made the figures and wrote the manuscript.

Funding

C.Z. acknowledges support provided by the XSEDE program under Grant TG-MAT200004. J.Y. acknowledges support from the US National Science Foundation (Grant No. 2038057) and Cornell University's faculty startup grant.

Notes

The authors declare no competing financial interest.

ACKNOWLEDGMENTS

C.L.M. and L.F.D. gratefully acknowledge the Department of Chemistry and Chemical Biology at Northeastern University. They thank Patrick A. Sullivan for his work on the illustrations in Figure ¹B and Figure S2. C.Z. acknowledges the computational resources from Florida State University.

ABBREVIATIONS

ECM, extracellular matrix; COL, collagen; PBS, phosphate-buffered saline; SEM, scanning electron microscopy; CG, coarse-grain; AA, all atomistic; LJ, Lennard-Jones; FN, fibronectin

■ REFERENCES

- (1) Frantz, C.; Stewart, K. M.; Weaver, V. M. The extracellular matrix at a glance. *J. Cell. Sci.* **2010**, 123 (Pt 24), 4195–200.
- (2) Hynes, R. O. The extracellular matrix: not just pretty fibrils. *Science* **2009**, 326 (5957), 1216–9.
- (3) Cowin, S. C. How is a Tissue Built? J. Biomech. Eng. 2000, 122, 553–569.
- (4) O'Brien, M. Structure and metabolism of tendons. Scand. J. Med. Sci. Sports 1997, 7 (2), 55–61.
- (5) Wren, T. A.; Yerby, S. A.; Beaupre, G. S.; Carter, D. R. Mechanical properties of the human achilles tendon. *Clin. Biomech.* (*Bristol, Avon*) **2001**, *16* (3), 245–51.
- (6) Boote, C.; Dennis, S.; Huang, Y.; Quantock, A. J.; Meek, K. M. Lamellar orientation in human cornea in relation to mechanical properties. *J. Struct. Biol.* **2005**, *149* (1), 1–6.
- (7) Holmes, D. F.; Gilpin, C. J.; Baldock, C.; Ziese, U.; Koster, A. J.; Kadler, K. E. Corneal collagen fibril structure in three dimensions: Structural insights into fibril assembly, mechanical properties, and tissue organization. *Proc. Natl. Acad. Sci. U. S. A.* **2001**, 98 (13), 7307–12
- (8) Hamilton, K. E.; Pye, D. C. Young's modulus in normal corneas and the effect on applanation tonometry. *Optom. Vis. Sci.* **2008**, 85 (6), 445–50.

- (9) Komai, Y.; Ushiki, T. The three-dimensional organization of collagen fibrils in the human cornea and sclera. *Invest. Ophthalmol. Vis. Sci.* **1991**, 32 (8), 2244–58.
- (10) Crichton, M. L.; Chen, X.; Huang, H.; Kendall, M. A. Elastic modulus and viscoelastic properties of full thickness skin characterised at micro scales. *Biomaterials* **2013**, 34 (8), 2087–97.
- (11) Yang, W.; Sherman, V. R.; Gludovatz, B.; Schaible, E.; Stewart, P.; Ritchie, R. O.; Meyers, M. A. On the tear resistance of skin. *Nat. Commun.* **2015**, *6*, 6649.
- (12) Kleinman, H. K.; Martin, G. R. Matrigel: Basement membrane matrix with biological activity. *Semin. Cancer Biol.* **2005**, *15* (5), 378–386
- (13) Nerger, B. A.; Brun, P.-T.; Nelson, C. M. Microextrusion printing cell-laden networks of type I collagen with patterned fiber alignment and geometry. *Soft Matter* **2019**, *15*, 5728.
- (14) Ghasemi-Mobarakeh, L.; Prabhakaran, M. P.; Morshed, M.; Nasr-Esfahani, M. H.; Ramakrishna, S. Bio-functionalized PCL nanofibrous scaffolds for nerve tissue engineering. *Mater. Sci. Eng.,* C 2010, 30 (8), 1129–1136.
- (15) Ejim, O. S.; Blunn, G. W.; Brown, R. A. Production of artificial-oriented mats and strands from plasma fibronectin: a morphological study. *Biomaterials* **1993**, *14*, 743.
- (16) Chantre, C. O.; Campbell, P. H.; Golecki, H. M.; Buganza, A. T.; Capulli, A. K.; Deravi, L. F.; Dauth, S.; Sheehy, S. P.; Paten, J. A.; Gledhill, K.; Doucet, Y. S.; Abaci, H. E.; Ahn, S.; Pope, B. D.; Ruberti, J. W.; Hoerstrup, S. P.; Christiano, A. M.; Parker, K. K. Production-scale fibronectin nanofibers promote wound closure and tissue repair in a dermal mouse model. *Biomaterials* **2018**, *166*, 96–108.
- (17) Chantre, C. O.; Gonzalez, G. M.; Ahn, S.; Cera, L.; Campbell, P. H.; Hoerstrup, S. P.; Parker, K. K. Porous Biomimetic Hyaluronic Acid and Extracellular Matrix Protein Nanofiber Scaffolds for Accelerated Cutaneous Tissue Repair. ACS Appl. Mater. Interfaces 2019, 11 (49), 45498–45510.
- (18) Buttafoco, L.; Kolkman, N. G.; Engbers-Buijtenhuijs, P.; Poot, A. A.; Dijkstra, P. J.; Vermes, I.; Feijen, J. Electrospinning of collagen and elastin for tissue engineering applications. *Biomaterials* **2006**, 27 (5), 724–734.
- (19) Paten, J. A.; Martin, C. L.; Wanis, J. T.; Siadat, S. M.; Figueroa-Navedo, A. M.; Ruberti, J. W.; Deravi, L. F. Molecular Interactions between Collagen and Fibronectin: A Reciprocal Relationship that Regulates De Novo Fibrillogenesis. *Chem.* **2019**, *5* (8), 2126–2145.
- (20) Martin, C. L.; Bergman, M. R.; Deravi, L. F.; Paten, J. A. A Role for Monosaccharides in Nucleation Inhibition and Transport of Collagen. *Bioelectricity* **2020**, 2 (2), 186–197.
- (21) Paten, J. A.; Siadat, S. M.; Susilo, M. E.; Ismail, E. N.; Stoner, J. L.; Rothstein, J. P.; Ruberti, J. W. Flow-Induced Crystallization of Collagen: A Potentially Critical Mechanism in Early Tissue Formation. ACS Nano 2016, 10 (5), 5027–40.
- (22) Holmes, D. F.; Yeung, C. C.; Garva, R.; Zindy, E.; Taylor, S. H.; Lu, Y.; Watson, S.; Kalson, N. S.; Kadler, K. E. Synchronized mechanical oscillations at the cell-matrix interface in the formation of tensile tissue. *Proc. Natl. Acad. Sci. U. S. A.* **2018**, *115* (40), E9288–E9297
- (23) Matthews, J. A.; Wnek, G. E.; Simpson, D. G.; Bowlin, G. L. Electrospinning of collagen nanofibers. *Biomacromolecules* **2002**, 3 (2), 232–8
- (24) Zhong, S.; Teo, W. E.; Zhu, X.; Beuerman, R. W.; Ramakrishna, S.; Yung, L. Y. An aligned nanofibrous collagen scaffold by electrospinning and its effects on in vitro fibroblast culture. *J. Biomed. Mater. Res., Part A* **2006**, *79* (3), 456–63.
- (25) Caves, J. M.; Kumar, V. A.; Wen, J.; Cui, W.; Martinez, A.; Apkarian, R.; Coats, J. E.; Berland, K.; Chaikof, E. L. Fibrillogenesis in continuously spun synthetic collagen fiber. *J. Biomed. Mater. Res. B Appl. Biomater.* **2010**, 93 (1), 24–38.
- (26) Yaari, A.; Schilt, Y.; Tamburu, C.; Raviv, U.; Shoseyov, O. Wet Spinning and Drawing of Human Recombinant Collagen. *ACS Biomater. Sci. Eng.* **2016**, *2*, 349–360.
- (27) Lee, A.; Hudson, A. R.; Shiwarski, D. J.; Tashman, J. W.; Hinton, T. J.; Yerneni, S.; Bliley, J. M.; Campbell, P. G.; Feinberg, A.

- W. 3D bioprinting of collagen to rebuild components of the human heart. *Science* **2019**, 365 (6452), 482–487.
- (28) Betsch, M.; Cristian, C.; Lin, Y. Y.; Blaeser, A.; Schoneberg, J.; Vogt, M.; Buhl, E. M.; Fischer, H.; Duarte Campos, D. F. Incorporating 4D into Bioprinting: Real-Time Magnetically Directed Collagen Fiber Alignment for Generating Complex Multilayered Tissues. Adv. Healthc. Mater. 2018, 7 (21), No. e1800894.
- (29) Zeugolis, D. I.; Khew, S. T.; Yew, E. S.; Ekaputra, A. K.; Tong, Y. W.; Yung, L. Y.; Hutmacher, D. W.; Sheppard, C.; Raghunath, M. Electro-spinning of pure collagen nano-fibres just an expensive way to make gelatin? *Biomaterials* **2008**, 29 (15), 2293–305.
- (30) Rogalski, J. J.; Bastiaansen, C. W. M.; Peijs, T. Rotary jet spinning review- a potential high yield future for polymer nanofibers. *Nanocomposites* **2017**, 3 (4), 97–121.
- (31) Bhardwaj, N.; Kundu, S. C. Electrospinning: a fascinating fiber fabrication technique. *Biotechnol. Adv.* **2010**, 28 (3), 325–47.
- (32) Saeidi, N.; Sander, E. A.; Ruberti, J. W. Dynamic shear-influenced collagen self-assembly. *Biomaterials* **2009**, *30* (34), 6581–92.
- (33) Lanfer, B.; Freudenberg, U.; Zimmermann, R.; Stamov, D.; Korber, V.; Werner, C. Aligned fibrillar collagen matrices obtained by shear flow deposition. *Biomaterials* **2008**, *29* (28), 3888–95.
- (34) Cheng, X.; Gurkan, U. A.; Dehen, C. J.; Tate, M. P.; Hillhouse, H. W.; Simpson, G. J.; Akkus, O. An electrochemical fabrication process for the assembly of anisotropically oriented collagen bundles. *Biomaterials* **2008**, 29 (22), 3278–88.
- (35) Torbet, J.; Ronziere, M. C. Magnetic alignment of collagen during self-assembly. *Biochem. J.* **1984**, *219* (3), 1057–9.
- (36) Saeidi, N.; Sander, E. A.; Zareian, R.; Ruberti, J. W. Production of highly aligned collagen lamellae by combining shear force and thin film confinement. *Acta Biomater.* **2011**, *7* (6), 2437–47.
- (37) Wilson, D. L.; Martin, R.; Hong, S.; Cronin-Golomb, M.; Mirkin, C. A.; Kaplan, D. L. Surface organization and nanopatterning of collagen by dip-pen nanolithography. *Proc. Natl. Acad. Sci. U. S. A.* **2001**, 98 (24), 13660–4.
- (38) Antman-Passig, M.; Shefi, O. Remote Magnetic Orientation of 3D Collagen Hydrogels for Directed Neuronal Regeneration. *Nano Lett.* **2016**, *16* (4), 2567–73.
- (39) Guo, C.; Kaufman, L. J. Flow and magnetic field induced collagen alignment. *Biomaterials* **2007**, 28 (6), 1105–14.
- (40) Zitnay, J. L.; Reese, S. P.; Tran, G.; Farhang, N.; Bowles, R. D.; Weiss, J. A. Fabrication of dense anisotropic collagen scaffolds using biaxial compression. *Acta Biomater.* **2018**, *65*, 76–87.
- (41) Hoogenkamp, H. R.; Bakker, G. J.; Wolf, L.; Suurs, P.; Dunnewind, B.; Barbut, S.; Friedl, P.; van Kuppevelt, T. H.; Daamen, W. F. Directing collagen fibers using counter-rotating cone extrusion. *Acta Biomater.* **2015**, *12*, 113–121.
- (42) Yang, S.; Shi, X.; Li, X.; Wang, J.; Wang, Y.; Luo, Y. Oriented collagen fiber membranes formed through counter-rotating extrusion and their application in tendon regeneration. *Biomaterials* **2019**, 207, 61–75.
- (43) Yang, S.; Wang, J.; Wang, Y.; Luo, Y. Key role of collagen fibers orientation in casing-meat adhesion. *Food Res. Int.* **2016**, 89 (Pt 1), 439–447.
- (44) Harper, B. A.; Barbut, S.; Lim, L.-T.; Marcone, M. F. Microstructural and textural investigation of various manufactured collagen sausage casings. *Food Res. Int.* **2012**, *49*, 494–500.
- (45) Depalle, B.; Qin, Z.; Shefelbine, S. J.; Buehler, M. J. Influence of cross-link structure, density and mechanical properties in the mesoscale deformation mechanisms of collagen fibrils. *J. Mech. Behav. Biomed. Mater.* **2015**, *52*, 1–13.
- (46) Buehler, M. J. Atomistic and continuum modeling of mechanical properties of collagen: elasticity, fracture, and self-assembly. J. Mater. Res. 2006, 21 (8), 1947–1961.
- (47) Gautieri, A.; Russo, A.; Vesentini, S.; Redaelli, A.; Buehler, M. J. Coarse-grained model of collagen molecules using an extended MARTINI force field. *J. Chem. Theory Comput.* **2010**, *6* (4), 1210–1218.

- (48) Zhang, N.; Cheng, Y.; Hu, X.; Yeo, J. Toward rational algorithmic design of collagen-based biomaterials through multiscale computational modeling. *Curr. Opin. Chem. Eng.* **2019**, 24, 79–87.
- (49) Buehler, M. J.; Wong, S. Y. Entropic elasticity controls nanomechanics of single tropocollagen molecules. *Biophys. J.* **2007**, 93 (1), 37–43.
- (50) Buehler, M. J. Nanomechanics of collagen fibrils under varying cross-link densities: atomistic and continuum studies. *J. Mech. Behav. Biomed. Mater.* **2008**, *1* (1), 59–67.
- (51) Buehler, M. J. Nature designs tough collagen: explaining the nanostructure of collagen fibrils. *Proc. Natl. Acad. Sci. U. S. A.* **2006**, 103 (33), 12285–12290.
- (52) Gautieri, A.; Buehler, M. J.; Redaelli, A. Deformation rate controls elasticity and unfolding pathway of single tropocollagen molecules. *J. Mech. Behav. Biomed. Mater.* **2009**, 2 (2), 130–137.
- (53) Depalle, B.; Qin, Z.; Shefelbine, S. J.; Buehler, M. J. Large deformation mechanisms, plasticity, and failure of an individual collagen fibril with different mineral content. *J. Bone Miner. Res.* **2016**, 31 (2), 380–390.
- (54) Sander, E. A.; Barocas, V. H. Comparison of 2D fiber network orientation measurement methods. *J. Biomed. Mater. Res., Part A* **2009**, 88 (2), 322–31.
- (55) Orgel, J. P.; Irving, T. C.; Miller, A.; Wess, T. J. Microfibrillar structure of type I collagen in situ. *Proc. Natl. Acad. Sci. U. S. A.* **2006**, 103 (24), 9001–9005.
- (56) Shoulders, M. D.; Raines, R. T. Collagen structure and stability. *Annu. Rev. Biochem.* **2009**, 78, 929–58.
- (57) Yong, C.; Higgs, P. Chain orientation in polymer networks: Computer simulations using the bond fluctuation model. *Macromolecules* **1999**, 32 (15), 5062–5071.
- (58) Liu, J.; Yang, R. Tuning the thermal conductivity of polymers with mechanical strains. *Phys. Rev. B: Condens. Matter Mater. Phys.* **2010**, *81* (17), 174122.
- (59) Allen, M. P.; Tildesley, D. J. Computer simulation of liquids; Oxford University Press: 2017.
- (60) Lai, E. S.; Anderson, C. M.; Fuller, G. G. Designing a tubular matrix of oriented collagen fibrils for tissue engineering. *Acta Biomater.* **2011**, *7* (6), 2448–56.
- (61) de Wild, M.; Pomp, W.; Koenderink, G. H. Thermal memory in self-assembled collagen fibril networks. *Biophys. J.* **2013**, *105* (1), 200–10.
- (62) Liu, G. Y.; Agarwal, R.; Ko, K. R.; Ruthven, M.; Sarhan, H. T.; Frampton, J. P. Templated Assembly of Collagen Fibers Directs Cell Growth in 2D and 3D. *Sci. Rep.* **2017**, *7*, 9628.
- (63) Kapoor, A.; Caporali, E. H. G.; Kenis, P. J. A.; Stewart, M. C. Microtopographically patterned surfaces promote the alignment of tenocytes and extracellular collagen. *Acta Biomater.* **2010**, *6*, 2580–2580
- (64) Kubow, K. E.; Vukmirovic, R.; Zhe, L.; Klotzsch, E.; Smith, M. L.; Gourdon, D.; Luna, S.; Vogel, V. Mechanical forces regulate the interactions of fibronectin and collagen I in extracellular matrix. *Nat. Commun.* **2015**, *6*, 8026.
- (65) Li, S.; Van Den Diepstraten, C.; D'Souza, S. J.; Chan, B. M.; Pickering, J. G. Vascular smooth muscle cells orchestrate the assembly of type I collagen via alpha2beta1 integrin, RhoA, and fibronectin polymerization. *Am. J. Pathol.* **2003**, *163* (3), 1045–56.